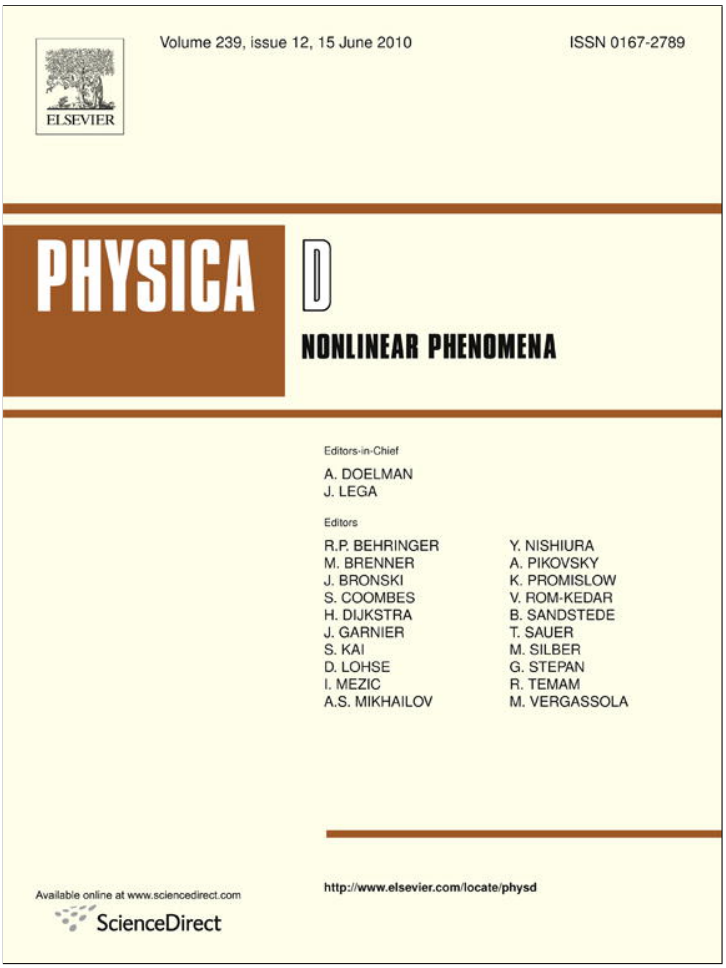

Physica D 239 (2010) 1048–1060

Contents lists available at ScienceDirect

Physica D

journal homepage: www.elsevier.com/locate/physd

Stability of bumps in piecewise smooth neural fields with nonlinear adaptation

Zachary P. Kilpatrick[a], Paul C. Bressloff[b,*]

[a] Department of Mathematics, University of Utah, Salt Lake City, UT 84112, USA
[b] Mathematical Institute, University of Oxford, 24-29 St. Giles', Oxford OX1 3LB, UK

ARTICLE INFO

Article history:
Received 7 December 2009
Received in revised form
23 February 2010
Accepted 25 February 2010
Available online 6 March 2010
Communicated by S. Coombes

Keywords:
Neural network
Synaptic depression
Spike frequency adaptation
Piecewise smooth dynamics

ABSTRACT

We study the linear stability of stationary bumps in piecewise smooth neural fields with local negative feedback in the form of synaptic depression or spike frequency adaptation. The continuum dynamics is described in terms of a nonlocal integrodifferential equation, in which the integral kernel represents the spatial distribution of synaptic weights between populations of neurons whose mean firing rate is taken to be a Heaviside function of local activity. Discontinuities in the adaptation variable associated with a bump solution means that bump stability cannot be analyzed by constructing the Evans function for a network with a sigmoidal gain function and then taking the high-gain limit. In the case of synaptic depression, we show that linear stability can be formulated in terms of solutions to a system of pseudo-linear equations. We thus establish that sufficiently strong synaptic depression can destabilize a bump that is stable in the absence of depression. These instabilities are dominated by shift perturbations that evolve into traveling pulses. In the case of spike frequency adaptation, we show that for a wide class of perturbations the activity and adaptation variables decouple in the linear regime, thus allowing us to explicitly determine stability in terms of the spectrum of a smooth linear operator. We find that bumps are always unstable with respect to this class of perturbations, and destabilization of a bump can result in either a traveling pulse or a spatially localized breather.

1. Introduction

Persistent, localized regions of neural activity have been proposed as substrates of several memory and sensory processes in the brain. Experiments in primate prefrontal cortex show that sensory cues can often lead to a spatially localized group of neurons persistently firing during a recall task. This "bump" of activity disappears once the task is complete [1–3]. Additionally, it has been suggested that the brain may keep the eyes still by representing eye position as an activity bump in the medial vestibular nucleus [4]. Also, visually evoked bumps of activity have been seen in striate cortex due to the orientation selectivity of recurrent connections [5]. There has been a great deal of work developing models that explain how such bumps of activity might arise and be sustained in a neuronal network [6–9]. One of the simplest models known to support stationary bumps is given by a scalar integrodifferential equation that represents averaged population activity in a spatially extended network of neurons [6]:

$$\tau \frac{\partial u(x,t)}{\partial t} = -u(x,t) + \int_{-\infty}^{\infty} w(x-x') f(u(x',t)-\theta)\mathrm{d}x' + I(x,t). \tag{1.1}$$

The variable $u(x,t)$ represents the local synaptic drive to a population of neurons at position x and time t, τ is the membrane time constant, $I(x,t)$ represents an external input, and $w(x)$ is a synaptic weight distribution. Usually w is a continuous function satisfying $w(-x) = w(x)$ and $\int_{-\infty}^{\infty} w(x)\mathrm{d}x < \infty$. The nonlinearity f denotes an output firing rate function. Typically, f is a bounded, positive monotone increasing function such as the sigmoid

$$f(u-\theta) = \frac{1}{1+\exp(-\eta(u-\theta))} \tag{1.2}$$

with gain η and threshold θ. Often, existence and stability of spatially localized solutions of Eq. (1.1) are conducted in the high-gain limit $\eta \to \infty$ such that f becomes the Heaviside function [6,9]

$$f(u-\theta) = \Theta(u-\theta) = \begin{cases} 0 & \text{if } u < \theta \\ 1 & \text{if } u > \theta. \end{cases} \tag{1.3}$$

It is then possible to establish existence of pulse solutions by explicit construction and to determine local stability in terms of an associated Evans function. The latter is obtained by linearizing the neural field equations about the pulse solution [10]. In the case of stationary pulses or bumps, local stability reduces to the problem of calculating the effects of perturbations at the bump boundary where $u(x) = \theta$.

Eq. (1.1) was first analyzed in detail by Amari [6], who showed that in the case of a Heaviside nonlinearity and a homogeneous input I the network can support a stable stationary bump solution

* Corresponding author. Tel.: +44 801 585 1633.
E-mail addresses: kilpatri@math.utah.edu (Z.P. Kilpatrick), bresslof@maths.ox.ac.uk (P.C. Bressloff).

0167-2789/$ – see front matter © 2010 Elsevier B.V. All rights reserved.
doi:10.1016/j.physd.2010.02.016

when the weight distribution $w(x)$ is given by a so-called Mexican hat function with the following properties: $w(x) > 0$ for $x \in [0, x_0)$ with $w(x_0) = 0$; $w(x) < 0$ for $x \in (x_0, \infty)$; $w(x)$ is decreasing on $[0, x_0]$; $w(x)$ has a unique minimum on $\mathbb{R}^+$ at $x = x_1$ with $x_1 > x_0$ and $w(x)$ strictly increasing on (x_1, ∞). On the other hand, in the case of a purely excitatory network with $w(x)$ a positive, monotonically decreasing function, any bump solution is unstable and tends to break up into a pair of counterpropagating fronts. Following Amari's original analysis, the study of bumps in neural fields has been extended to multiple bump solutions in networks with oscillatory weight functions [11,12], two-dimensional bumps [13,12,14–16], and weakly interacting bumps [17]. There has also been some progress in studying the existence of bumps in scalar neural fields when the firing rate function is continuous in both infinite [18,19] and compact spatial domains [20].

One limitation of the scalar neural field model given by Eq. (1.1) is that it cannot support traveling pulses nor spatially structured oscillations when inhibition is blocked, which is inconsistent with a variety of *in vitro* experimental studies of disinhibited slice preparations [21]. These more complex forms of spatiotemporal dynamics can occur, however, when some of form of local negative feedback is included [22–27]. Pinto and Ermentrout proposed a neural field model with linear negative feedback that is analogous to the recovery variable in the Fitzhugh–Nagumo equation [22,19]. The existence and stability of stationary bumps can then be studied using a straightforward extension of the Amari analysis, since the bump solution is smooth in a neighborhood of the threshold crossing points. However, the analysis of bump stability is more complicated in the case of nonlinear forms of negative feedback such as synaptic depression [26] and spike frequency adaptation [23,25]. In these models, the amplitude of the feedback depends on the firing rate so if the latter is taken to be a Heaviside function, then the resulting dynamical system becomes piecewise smooth. In particular, it is no longer possible to determine stability by directly linearizing the neural field equations about a bump solution. Previous studies have thus constructed an Evans function for bump stability by linearizing the neural field equations with a smooth sigmoid (1.2) and then taking the high-gain limit [23,25,26]. However, the size of perturbations for which the linear theory remains valid vanishes in the high-gain limit, so that the Evans function approach does not fully capture the piecewise nature of the dynamics. Indeed, it is well known from the theory of piecewise smooth ordinary differential equations that fixed point solutions can abruptly appear or disappear, and the stability of a fixed point often depends on the properties of a piecewise linear operator [28].

In this paper, we follow a different approach to analyzing bump stability, in which the piecewise smooth nature of the dynamics in the high-gain limit is explicitly taken into account. It turns out that the way in which the piecewise smooth dynamics affects bump stability is strongly model dependent. In order to illustrate this, we study the linear stability of bumps in two different neural networks with piecewise smooth local negative feedback. In Section 2, bumps in a network with synaptic depression are examined. We first demonstrate that an Evans function approach is singular in the high-gain limit and underestimates the ability of synaptic depression to destabilize a bump. We then show how the linear stability of a bump can be analyzed in terms of solutions to a system of pseudo-linear equations, and use this to derive sufficient conditions for the instability of a bump. In the particular case of a network with a Mexican hat weight distribution, we show that sufficiently strong synaptic depression destabilizes a bump that is stable in the absence of depression. In Section 3, we study bumps in a network with spike frequency adaptation, which appears as a dynamic threshold in the firing rate function f. As with the network with depression, an Evans function approach breaks down in the high-gain limit, and we must resort to specifically addressing piecewise smoothness in stability calculations. In this case, we show that for a wide class of infinitesimal perturbations the activity and adaptation variables decouple in the linear regime, such that stability with respect to these perturbations can be determined using a straightforward modification of the standard Amari spectral equation [6]. We find that, in contrast to the stability analysis based on the high-gain limit of an Evans function [23,25], all bumps in the network are unstable, regardless of the strength of adaptation.

2. Neural network with synaptic depression

In this section, we analyze the existence and local stability of stationary bumps in a one-dimensional neural field model with synaptic depression. Synaptic depression is the process by which presynaptic resources such as chemical neurotransmitter or synaptic vesicles are depleted [29]. It can be incorporated into the scalar neural field model [6] by introducing a dynamic prefactor q in the nonlocal term according to [26,27]

$$\tau \frac{\partial u(x,t)}{\partial t} = -u(x,t) + \int_{-\infty}^{\infty} q(x',t) w(x-x') f(u(x',t)-\theta) \mathrm{d}x', \tag{2.1a}$$

$$\frac{\partial q(x,t)}{\partial t} = \frac{1-q(x,t)}{\alpha} - \beta q(x,t) f(u(x,t)-\theta). \tag{2.1b}$$

The factor $q(x,t)$ can be interpreted as a measure of the fraction of available presynaptic resources, which are depleted at a rate βf [30,31], and are recovered on a timescale specified by the constant α (experimentally shown to be 200–800 ms [32,33,30]). If we assume that the strength of a synapse is reduced by a factor $\eta = 0.05 - 0.9$ of its maximal value in response to a sustained input of rate $f = 1$ [32], then a simple steady-state calculation shows that $\beta \approx (1-\eta)/(\eta\alpha) \approx 0.0001 - 0.1\ (\mathrm{ms})^{-1}$ for the given range of values of α. If we take $f = \Theta$ then the dynamics becomes piecewise smooth due to the presence of the Heaviside function Θ in the dynamical equation for the depression variable $q(x,t)$. In the following we set the time constant $\tau = 1$ which sets the unit of time to be of the order 10 ms.

2.1. Existence of bumps

On setting $f = \Theta$, a stationary solution $(U(x), Q(x))$ of Eq. (2.1) satisfies the pair of equations

$$U(x) = \int_{-\infty}^{\infty} Q(x') w(x-x') \Theta(U(x')-\theta) \mathrm{d}x', \tag{2.2}$$

$$Q(x) = 1 - \frac{\alpha\beta}{1+\alpha\beta} \Theta(U(x)-\theta). \tag{2.3}$$

Let $R[U] = \{x | U(x) > \theta\}$ be the region over which the field is excited or superthreshold. Exploiting the fact that any solution can be arbitrarily translated along the x-axis, we define a stationary bump solution of half-width a to be one for which $R[U] = (-a, a)$. Substituting Eq. (2.3) into (2.2) then yields

$$U(x) = \frac{1}{1+\alpha\beta}[W(x+a) - W(x-a)], \qquad W(x) = \int_0^x w(y)\mathrm{d}y. \tag{2.4}$$

As a simple example, we take a Mexican hat weight distribution given by the function

$$w(x) = (1-|x|)\mathrm{e}^{-|x|}, \tag{2.5}$$

which models short-range excitation and long-range inhibition as a function of distance in the connections between neural populations. Substituting the weight function (2.5) into the steady

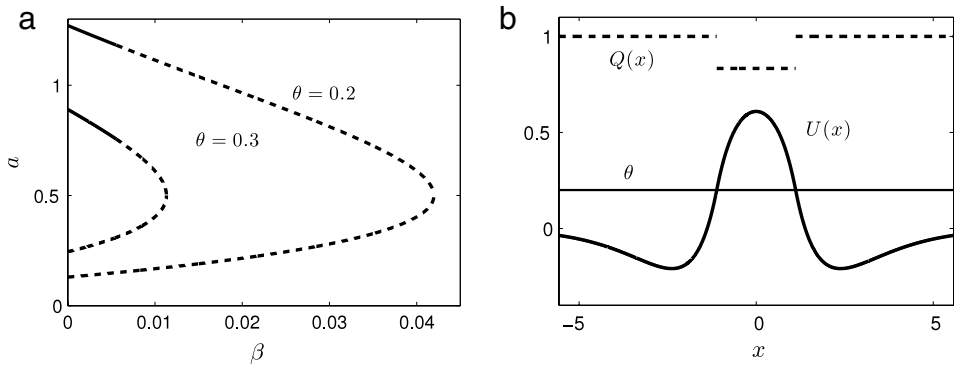

Fig. 1. Stationary bumps in a network with synaptic depression. (a) Plots relating bump width a to amplitude of synaptic depression β for different values of θ using Eq. (2.6). We take the parameter $\alpha = 20$. Stability analysis based on the piecewise smooth approach (Section 2.3) establishes that bumps along the dashed portions of the existence curves are unstable; the solid curves indicate bumps that appear to be numerically stable. The Evans function approach predicts that the whole of the upper branch is stable. (b) Bump profile when $\theta = 0.2$ and $\beta = 0.01$.

state solution for $U(x)$ and evaluating the integral yields

$$U(x) = \frac{1}{(1+\alpha\beta)}\left[(x+a)e^{-|x+a|} - (x-a)e^{-|x-a|}\right].$$

Applying the threshold conditions $U(\pm a) = \theta$, we arrive at an implicit expression relating the bump half-width a to all other parameters:

$$\frac{2a}{(1+\alpha\beta)}e^{-2a} = \theta.$$

The transcendental equation (2.6) can be solved numerically using a root finding algorithm. The variation of pulse width with the parameters θ and β is shown in Fig. 1; the stability of the bumps is calculated below. It is important to note that the threshold-crossing conditions (2.6) are necessary but not sufficient for existence of a bump. A rigorous proof of existence, which establishes that activity is superthreshold everywhere within the domain $|x| < a$ and subthreshold for all $|x| > a$, has not been obtained except in special cases [6]. However, it is straightforward to check numerically that these conditions are satisfied.

2.2. Stability of bumps: Evans function approach

A popular approach to analyzing the stability of stationary bumps in neural field models is to linearize about the bump solution and derive an Evans function, whose roots represent the spectrum of the associated linear system [10]. Thus, it is tempting to try to calculate the Evans function of the bump solutions (2.6), find its roots, and use these to make statements about the linear stability of the bump. However, the steps necessary to linearize the system (2.1) when $f = \Theta$ are not well defined, due to the exposed Heaviside function in Eq. (2.1b). This suggests that one way to proceed is to take f to be the sigmoid function (1.2) with high gain ($\eta \gg 1$), formally construct the associated Evans function by Taylor expanding about the bump solution and then take the high-gain limit $\eta \to \infty$ to recover the Evans function in the case of the Heaviside. (One cannot evaluate the Evans function analytically for a smooth sigmoid, since one does not have an explicit expression for the bump solution.) However, in the high-gain limit the region of phase space in which the linear stability theory is valid becomes vanishingly small, due to the ever steepening slope of the sigmoid right at the threshold crossing points. Thus, it is not clear that the resulting Evans function will correctly characterize the linear stability of the bump. Nonetheless, it is useful to present such a construction here and to point out how it breaks down in the high-gain limit, leading to erroneous stability results.

We begin by letting $u(x,t) = U_\eta(x) + \epsilon\psi(x,t)$ and $q(x,t) = Q_\eta(x) + \epsilon\varphi(x,t)$, where ψ, φ are smooth perturbations, $\epsilon \ll 1$, and the pair (U_η, Q_η) denotes a stationary bump solution of Eq. (2.1) for a smooth sigmoid function f with gain η. Substituting into the full system (2.1), expanding to first order in ϵ and imposing the stationary bump solutions yields the linear equations

$$\frac{\partial\psi(x,t)}{\partial t} = -\psi(x,t) + \int_{-\infty}^{\infty} w(x-x')\Big\{Q_\eta(x') \times f'(U_\eta(x')-\theta)\psi(x',t) + \varphi(x',t)f(U_\eta(x')-\theta)\Big\}dx' \tag{2.6}$$

$$\frac{\partial\varphi(x,t)}{\partial t} = -\frac{\varphi(x,t)}{\alpha} - \beta\Big[Q_\eta(x)f'(U_\eta(x)-\theta)\psi(x,t) + \varphi(x,t)f(U_\eta(x)-\theta)\Big]. \tag{2.7}$$

We have used the Taylor series approximation

$$f(U_\eta + \psi - \theta) = f(U_\eta - \theta) + f'(U_\eta - \theta)\psi + \cdots. \tag{2.8}$$

Notice that

$$f'(U_\eta(x)-\theta) = \frac{\eta\exp(-\eta(U_\eta(x)-\theta))}{(1+\exp(-\eta(U_\eta(x)-\theta)))^2} \tag{2.9}$$

is well defined when $U_\eta(x) \neq \theta$ as $\eta \to \infty$. However, when $U_\eta(x) = \theta$, which is where we define threshold crossings in the high-gain limit, Eq. (2.9) scales linearly with η. This will invalidate any linear approximation to f in the vicinity of a threshold crossing. Along these lines, as the high-gain limit is approached, for steeper and steeper sigmoids, the linear approximation at the threshold crossing becomes progressively worse. Thus, there is a vanishingly small region of the phase space $(\psi(x,t), \varphi(x,t))$ in which this stability analysis will be valid. Therefore, although one can formally analyze the high-gain limit of the spectrum of the smooth linear operator defined by the right-hand side of Eqs. (2.6) and (2.7), this does not yield valid conditions for linear stability of a bump in a network with Heaviside nonlinearities. Nevertheless, it is instructive to carry out the spectral analysis of Eqs. (2.6) and (2.7). That is, set $\psi(x,t) = e^{\lambda t}\psi(x)$ and $\varphi(x,t) = e^{\lambda t}\varphi(x)$ with $(\psi(x), \varphi(x))$ bounded continuous functions on $\mathbb{R}$ that decay to zero exponentially as $x \to \pm\infty$. This gives

$$(\lambda+1)\psi(x) = \int_{-\infty}^{\infty} w(x-x')\Big\{Q_\eta(x')\psi(x')f'(U_\eta(x')-\theta) + \varphi(x')f(U_\eta(x')-\theta)\Big\}dx', \tag{2.10}$$

$$(\lambda+\alpha^{-1})\varphi(x) = -\beta\Big[Q_\eta(x)\psi(x)f'(U_\eta(x)-\theta) + \varphi(x)f(U_\eta(x)-\theta)\Big]. \tag{2.11}$$

The resulting spectral problem is nontrivial since we have a non-compact linear operator on $\mathbb{R}$. However, we can obtain a simpler spectral problem by formally taking the high-gain limit.

First, solving Eq. (2.11) for $\varphi(x)$ yields

$$\varphi(x) = -\beta(\lambda+\alpha^{-1} + \beta f(U_\eta(x)-\theta))^{-1} Q_\eta(x)\psi(x) f'(U(x)-\theta). \tag{2.12}$$

Assuming that $\varphi(x)$ is non-singular, we may substitute back into Eq. (2.10) to give a closed equation for $\psi(x)$

$$(\lambda+1)\psi(x) = \int_{-\infty}^{\infty} w(x-x')Q_\eta(x')\psi(x')\Big\{f'(U(x')-\theta) - \beta\left(\lambda+\alpha^{-1}+\beta f(U_\eta(x')-\theta)\right)^{-1} \times f(U_\eta(x')-\theta)f'(U(x')-\theta)\Big\}\mathrm{d}x'. \tag{2.13}$$

We now take the high-gain limit using

$$\lim_{\eta\to\infty} f(U_\eta(x)-\theta) = \Theta(U(x)-\theta) = \Theta(x+a)-\Theta(x-a),$$

$$\lim_{\eta\to\infty} f'(U_\eta(x)-\theta) = \Theta'(U(x)-\theta) = \frac{\delta(x+a)}{|U'(a)|} + \frac{\delta(x-a)}{|U'(a)|},$$

$$\lim_{\eta\to\infty} f(0) = 1/2,$$

$$\lim_{\eta\to\infty} Q_\eta(\pm a) = \frac{1+\alpha\beta/2}{1+\alpha\beta}$$

so that Eq. (2.13) becomes [26]

$$\left(\lambda+\alpha^{-1}+\frac{\beta}{2}\right)(\lambda+1)\psi(x) = \frac{(\lambda+\alpha^{-1})(1+\alpha\beta/2)}{(1+\alpha\beta)|U'(a)|} \times [w(x+a)\psi(-a)+w(x-a)\psi(a)]. \tag{2.14}$$

Eq. (2.14) may appear to be a perfectly reasonable equation for characterizing the linear stability of a bump in a Heaviside network, due to its similarity to previous studies of the scalar equation (1.1). Indeed, one can determine λ in terms of the spectrum of the linear operator $\mathcal{L}\psi(x) = w(x+a)\psi(-a)+w(x-a)\psi(a)$ acting on the space of continuous bounded functions on $[-a,a]$; it can be shown that the linear operator is compact in the case of standard norms such as L^1 [34,35]. It then follows that the essential spectrum is located at $\lambda=-1$ and the discrete spectrum is determined by setting $x=\pm a$ in Eq. (2.14). This yields two classes of eigenfunctions $\psi_\pm(x) = w(x+a)\pm w(x-a)$ with associated characteristic equations [26]

$$\left(\lambda+\alpha^{-1}+\frac{\beta}{2}\right)(\lambda+1) = \Omega_\pm(\lambda+\alpha^{-1})(1+\alpha\beta/2), \tag{2.15}$$

where $\Omega_+=\Omega$, $\Omega_-=1$ with

$$\Omega = \frac{w(0)+w(2a)}{w(0)-w(2a)}. \tag{2.16}$$

It is straightforward to show that the characteristic equation for $\psi_-(x)$ has a simple root $\lambda_-=0$; one expects a zero eigenvalue, since this is an indication of the full system of Eqs. (2.1) being invariant with respect to spatial translations. However, although one can formally take the high-gain limit of the linear equation (2.13), this does not properly take into account the breakdown in the Taylor expansion of the full equations due to the singularity arising on the steepest part of the sigmoid. Consequently, the Evans function approach misses instabilities arising from the piecewise smooth nature of the full system (2.1). Indeed, the Evans function approach implies that the upper branch of the existence curve shown in Fig. 1 is linearly stable, that is, all non-zero solutions of (2.15) have negative real part along this branch, whereas at least some of this branch is unstable according to the piecewise smooth approach and according to numerical simulations (see below).

2.3. Stability of bumps: piecewise smooth approach

Rather than analyzing stability in terms of the high-gain limit of an Evans function, we now consider directly the effects of infinitesimal perturbations on a stationary bump solution of Eq. (2.1) when $f=\Theta$. Substituting $u(x,t)=U(x)+\epsilon\psi(x,t)$ and $q(x,t)=Q(x)+\epsilon\varphi(x,t)$ into the full system (2.1), imposing the stationary bump solutions (2.2) and (2.3), and dividing through by ϵ then gives

$$\frac{\partial\psi(x,t)}{\partial t} = -\psi(x,t) + \frac{1}{\epsilon}\int_{-\infty}^{\infty} w(x-x')Q(x') \times \left[\Theta(U(x')+\epsilon\psi(x',t)-\theta)-\Theta(U(x')-\theta)\right]\mathrm{d}x' + \int_{-\infty}^{\infty} w(x-x')\varphi(x',t)\Theta(U(x') + \epsilon\psi(x',t)-\theta)\mathrm{d}x' \tag{2.17}$$

$$\frac{\partial\varphi(x,t)}{\partial t} = -\frac{\varphi(x,t)}{\alpha} - \frac{\beta}{\epsilon}Q(x)\Big[\Theta(U(x)+\epsilon\psi(x,t)-\theta) - \Theta(U(x)-\theta)\Big] - \beta\varphi(x,t)\Theta(U(x)+\epsilon\psi(x,t)-\theta). \tag{2.18}$$

Denote the perturbations of the bump boundary by $\epsilon\Delta_\pm(t)$ such that

$$u(a+\epsilon\Delta_+(t),t) = u(-a+\epsilon\Delta_-(t),t) = \theta$$

for all $t>0$. Taylor expanding these threshold conditions to first order in ϵ we find that

$$\Delta_\pm(t) \approx \pm\frac{\psi(\pm a,t)}{|U'(a)|}. \tag{2.19}$$

We can smooth out the discontinuities in Eq. (2.18) by introducing the field

$$\Phi(x,t) = \int_{-a+\epsilon\Delta_-(t)}^{a+\epsilon\Delta_+(t)} w(x-x')\varphi(x',t)\mathrm{d}x'. \tag{2.20}$$

(We will not be able to perform such a change of variables in the case of the network with spike frequency adaptation in Section 3.) That is, infinitesimal shifts in the location of the bump boundary lead to $\mathcal{O}(1/\epsilon)$ pointwise changes in the perturbations $\varphi(x,t)$ over a time-scale of α^{-1}. However, this doesn't necessarily imply that the bump solution is unstable, since the region over which the $\mathcal{O}(1/\epsilon)$ changes occur may shrink to zero. This is captured by the dynamics of the field $\Phi(x,t)$, which will remain $\mathcal{O}(1)$ when $\varphi(x,t)$ is $\mathcal{O}(1/\epsilon)$ over an infinitesimal interval.

Differentiating Eq. (2.20) with respect to t and combining this with Eqs. (2.17) and (2.18) gives

$$\frac{\partial\psi(x,t)}{\partial t} = -\psi(x,t)+\Phi(x,t) + \frac{1}{\epsilon}\int_{-a+\epsilon\Delta_-(t)}^{a+\epsilon\Delta_+(t)} w(x-x')Q(x')\mathrm{d}x' - \frac{1}{\epsilon}\int_{-a}^{a} w(x-x')Q(x')\mathrm{d}x' \tag{2.21}$$

$$\frac{\partial\Phi(x,t)}{\partial t} = -\left(\alpha^{-1}+\beta\right)\Phi(x,t) - \frac{\beta}{\epsilon}\int_{-a+\epsilon\Delta_-(t)}^{a+\epsilon\Delta_+(t)} w(x-x')Q(x') \times [\Theta(U+\epsilon\psi-\theta)-\Theta(U-\theta)]\mathrm{d}x' + \epsilon w(x-a-\epsilon\Delta_+(t))\varphi(a+\epsilon\Delta_+(t),t)\dot{\Delta}_+(t) - \epsilon w(x+a-\epsilon\Delta_-(t))\varphi(-a+\epsilon\Delta_-(t),t)\dot{\Delta}_-(t). \tag{2.22}$$

We can now linearize Eqs. (2.21) and (2.22) by expanding in powers of ϵ and collecting all $\mathcal{O}(1)$ terms. Note that it is important to keep track of the signs of $\Delta_\pm$ when approximating the various

integrals due to the discontinuous nature of $Q(x)$. We thus obtain the following pseudo-linear system of equations:

$$\frac{\partial \psi(x,t)}{\partial t} = -\psi(x,t) + \Phi(x,t) + \gamma w(x+a)\psi(-a,t) \times G(\psi(-a,t)) + \gamma w(x-a)\psi(a,t)G(\psi(a,t)) \tag{2.23}$$

$$\frac{\partial \Phi(x,t)}{\partial t} = -\left(\alpha^{-1}+\beta\right)\Phi(x,t) - \beta\gamma w(x+a)\psi(-a,t)G(\psi(-a,t))\Theta(\psi(-a,t)) - \beta\gamma w(x-a)\psi(a,t)G(\psi(a,t))\Theta(\psi(a,t)), \tag{2.24}$$

where G is the step function

$$G(\Delta) = \begin{cases} 1 & \text{if } \Delta > 0 \\ (1+\alpha\beta)^{-1} & \text{if } \Delta < 0, \end{cases} \tag{2.25}$$

and

$$\gamma^{-1} = U'(-a) = -U'(a) = \frac{w(0)-w(2a)}{1+\alpha\beta}. \tag{2.26}$$

Eqs. (2.23) and (2.24) imply that the local stability of a stationary bump solution depends on the solutions to a system of pseudo-linear equations. A class of solutions to these equations can be obtained under the ansatz that the perturbations $\psi(\pm a,t)$ (or equivalently $\Delta_\pm(t)$) do not switch sign for any time t. In other words, we assume that Eqs. (2.23) and (2.24) have separable solutions of the form $(\psi(x,t),\Phi(x,t)) = \mathrm{e}^{\lambda t}(\psi(x),\Phi(x))$, where λ is real and $(\psi(x),\Phi(x))$ are bounded continuous functions on $\mathbb{R}$ that decay to zero exponentially as $x \to \pm\infty$. Under this assumption, the step functions Θ, G are time-independent so that there is a common factor $\mathrm{e}^{\lambda t}$ that cancels everywhere. We thus obtain

$$(\lambda+1)\psi(x) = \gamma w(x+a)\psi(-a)G(\psi(-a))\left(1-\frac{\beta\Theta(\psi(-a))}{\lambda+\alpha^{-1}+\beta}\right) + \gamma w(x-a)\psi(a)G(\psi(a))\left(1-\frac{\beta\Theta(\psi(a))}{\lambda+\alpha^{-1}+\beta}\right). \tag{2.27}$$

Note that we are assuming that $\lambda \neq -(\alpha^{-1}+\beta)$ so that we can use Eq. (2.23) to solve $\Phi(x)$ in terms of $\psi(\pm a)$; the case $\lambda = -(\alpha^{-1}+\beta)$ does not contribute to any instabilities.

Hence, in the case of the neural field with synaptic depression, the piecewise smooth nature of the full system persists in the pseudo-linear system characterizing the stability of bumps. This is an indication that the discontinuities arising in the stationary bump solution are manageable by linear stability analysis under the appropriate change of variables (2.20). By generalizing the analysis of Guo and Chow [35], it is possible to show how the solutions for λ can be identified with the spectra of a set of compact linear operators acting in the space of bounded continuous functions on the interval $[-a,a]$ [36]. However, here it will suffice to calculate λ directly from Eq. (2.27). One particular class of solutions consists of functions $\psi(x)$ that vanish on the boundary, $\psi(\pm a) = 0$, such that $\lambda = -1$. This determines the essential spectrum, since $\lambda = -1$ has infinite multiplicity, and does not contribute to any instabilities. There are then four other classes of solution to Eq. (2.27) which determine the discrete spectrum: (i) $\psi(-a) > 0$ and $\psi(a) < 0$; (ii) $\psi(-a) < 0$ and $\psi(a) > 0$; (iii) $\psi(-a) > 0$ and $\psi(a) > 0$; (iv) $\psi(-a) < 0$ and $\psi(a) < 0$. The four types of perturbation correspond, respectively, to a leftward shift, a rightward shift, an expansion, and a contraction of the stationary bump solution.

(i) $\psi(\pm a) \lesseqgtr 0$: in this case Eq. (2.27) becomes

$$\left(\lambda+\alpha^{-1}+\beta\right)(\lambda+1)\psi(x) = \gamma w(x+a)\psi(-a)\left(\lambda+\alpha^{-1}\right) + \gamma w(x-a)\psi(a)\frac{\lambda+\alpha^{-1}+\beta}{1+\alpha\beta}. \tag{2.28}$$

Setting $x = \pm a$ then yields the matrix equation

$$\begin{pmatrix} \Gamma_\beta(\lambda) - \gamma w(0)\left(\lambda+\alpha^{-1}\right) & -\gamma\left(\lambda+\alpha^{-1}\right)w(2a) \\ -\gamma\left(\lambda+\alpha^{-1}\right)w(2a) & \Gamma_\beta(\lambda) - \gamma w(0)\left(\lambda+\alpha^{-1}\right) \end{pmatrix} \times \begin{pmatrix} \psi(-a) \\ \psi(a) \end{pmatrix} = -\frac{\gamma\alpha\beta\lambda}{1+\alpha\beta}\begin{pmatrix} w(2a)\psi(a) \\ w(0)\psi(a) \end{pmatrix}, \tag{2.29}$$

where

$$\Gamma_\beta(\lambda) = \left(\lambda+\alpha^{-1}+\beta\right)(\lambda+1).$$

We thus obtain a quartic equation for λ. It is straightforward to show that there exists a zero eigenvalue $\lambda = 0$ with corresponding eigenmode $\psi(-a) = -\psi(a) > 0$, which represents a leftward shift. The existence of a zero eigenvalue reflects the translation invariance of the full system (2.1). Notice that we are able to pick up the translation invariance of the bump in our perturbation analysis, even though modifications necessary to shift $Q(x)$ in space will be $\mathcal{O}(1)$ in a neighborhood of $x = \pm a$. This is a consequence of introducing the field Φ according to Eq. (2.20), which remains small under small shifts in the bump. (As previously mentioned, such a technique will not be possible for the adaptive network in Section 3, so we will not witness the translation invariance of the system in the linear stability equations.) In order to calculate any other eigenvalues, we assume that $\beta \ll 1$ (which is consistent with physiological values for the depletion rate of synaptic depression [30,31]) and carry out a perturbation expansion in β. First, setting $\beta = 0$ in Eq. (2.29) we find that there are three eigenvalues $\lambda_0 = \Omega - 1, 0, -\alpha^{-1}$ with Ω given by Eq. (2.16). The first eigenvalue is $\lambda_0 = \Omega - 1$, which can be excluded since the corresponding eigenmode violates the assumption that $\psi(\pm a)$ have opposite sign; the associated solution branch for $\beta > 0$ can also be excluded. The second eigenvalue is $\lambda_0 = 0$, which persists when $\beta > 0$ (see above). Finally, the third eigenvalue $\lambda_0 = -\alpha^{-1}$ is doubly degenerate so that one needs to use degenerate perturbation theory in order to determine the splitting of the eigenvalue into two branches as β increases from zero; λ is a continuous function of β on both branches. Again, one of the branches is excluded by requiring that $\psi(\pm a)$ have opposite sign. We conclude that for sufficiently small β, shift perturbations do not lead to any instabilities.

(ii) $\psi(\pm a) \gtrless 0$: as expected from the reflection symmetry of the original system (2.1) when $w(x)$ is an even function, the spectrum associated with rightward shifts is identical to that of leftward shifts.

(iii) $\psi(\pm a) > 0$: in this case Eq. (2.27) becomes

$$\left(\lambda+\alpha^{-1}+\beta\right)(\lambda+1)\psi(x) = \gamma w(x+a)\psi(-a)\left(\lambda+\alpha^{-1}\right) + \gamma w(x-a)\psi(a)\left(\lambda+\alpha^{-1}\right). \tag{2.30}$$

Setting $x = \pm a$ and noting that $\psi(\pm a)$ have the same sign, we have $\psi(a) = \psi(-a) > 0$ with λ satisfying the quadratic equation

$$\left(\lambda+\alpha^{-1}+\beta\right)(\lambda+1) = \left(\lambda+\alpha^{-1}\right)(1+\alpha\beta)\Omega, \tag{2.31}$$

where Ω is given by Eq. (2.16) and we have substituted for γ using Eq. (2.26). It follows that $\lambda = \lambda_\pm$ with

$$\lambda_\pm = \frac{1}{2}\left[\Omega(1+\alpha\beta) - \left(1+\alpha^{-1}+\beta\right)\right] \pm \frac{1}{2}\sqrt{\left[\Omega(1+\alpha\beta) - \left(1+\alpha^{-1}+\beta\right)\right]^2 + 4(\Omega-1)\left(\alpha^{-1}+\beta\right)}. \tag{2.32}$$

The associated eigenmode corresponds to an expansion of the bump.

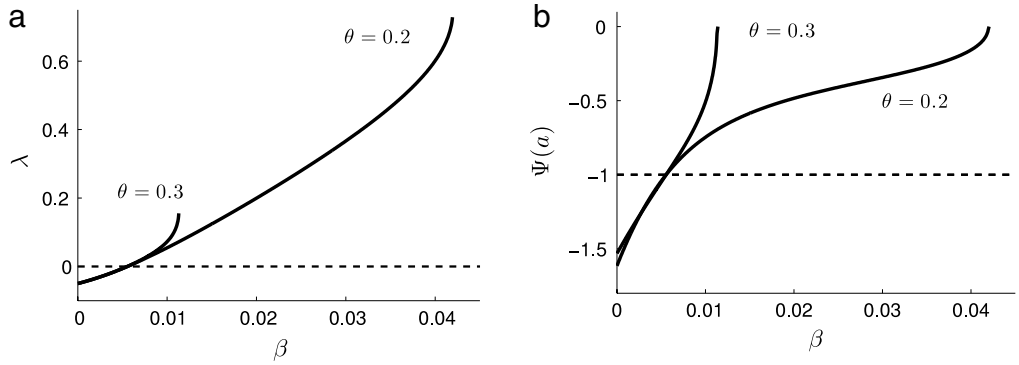

Fig. 2. Eigenvalues associated with respect to shift perturbations (cases (i) and (ii)). (a) Nonzero eigenvalue for various β. Bump is unstable with respect to shifts for sufficiently large β. The point at which λ becomes positive is slightly different for the two curves. (b) Corresponding plot of the ratio $\Psi(a) = \psi(a)/\psi(-a)$ for a leftward shift. As β increases, the ratio approaches zero. We take the parameter $\alpha = 20$. Results are the same for a rightward shift on exchanging $x = -a$ and $x = a$.

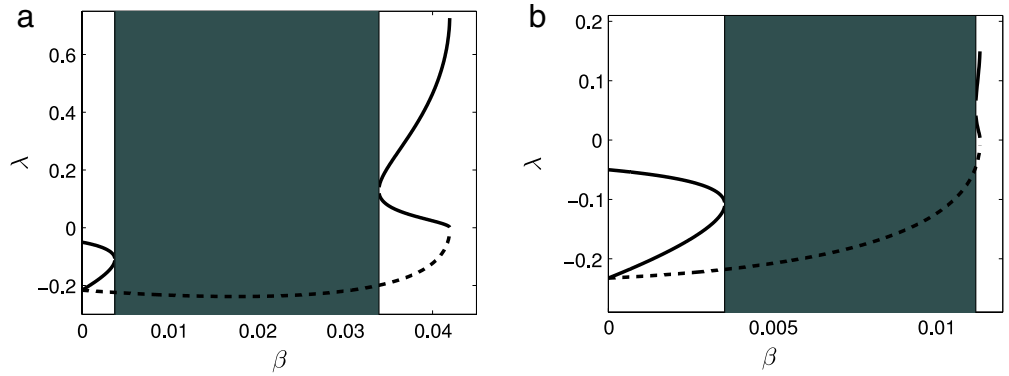

Fig. 3. Eigenvalues associated with expansion and contraction perturbations (cases (iii) and (iv)). (a) Eigenvalues of the expansion (solid curves) and contraction (dashed curve) perturbations when (a) $\theta = 0.2$ and (b) $\theta = 0.3$. In the grey regions, the roots of Eq. (2.32) are complex thus violating the ansatz that λ is real. We take $\alpha = 20$.

(iv) $\psi(\pm a) < 0$: in this final case Eq. (2.27) becomes

$$(\lambda+1)\psi(x) = \gamma w(x+a)\psi(-a)\frac{1}{1+\alpha\beta} + \gamma w(x-a)\psi(a)\frac{1}{1+\alpha\beta}. \tag{2.33}$$

Setting $x = \pm a$ shows that $\psi(a) = \psi(-a)$ and $\lambda = \lambda_0$ with

$$\lambda_0 = \Omega - 1. \tag{2.34}$$

The associated eigenmode corresponds to a contraction of the bump.

We now illustrate an application of the above stability analysis by considering stationary bumps in a network with the Mexican hat weight function (2.5). Specifically, we plot the real eigenvalues for each type of perturbation in the case of the wider bump shown in Fig. 1, which is stable in the absence of synaptic depression ($\beta = 0$). In Fig. 2, we plot the nonzero eigenvalue λ for shift perturbations as a function of β; the other two non-zero solutions to the matrix equation (2.29) violate the shift restriction $\psi(a) < 0 < \psi(-a)$. As β increases, the eigenvalue becomes positive, representing destabilization with respect to a shift perturbation. In comparison, the eigenvalues of type (iii) and (iv) perturbations (expansions and contractions) are plotted in Fig. 3. As β is increased, the eigenvalues of the expansion perturbation become positive, whereas the contraction perturbation is always stable for the chosen parameters. Since the expansion instability occurs at larger values of β than shift perturbations, the latter dominate bump instabilities in the case of the given Mexican hat weight function. Numerical simulations show that the resulting instability leads to the formation of a traveling pulse similar to that shown in Fig. 9 for a network with spike frequency adaptation. Another important point is that there exists a parameter range where eigenvalues (2.32) are complex, so stability of expanding perturbations cannot be analyzed using our given ansatz. When real roots appear again, there is a jump in their value. Note that the lower positive branch of expansion eigenvalues meets the branch of contraction eigenvalues at the critical value of β for which the upper and lower existence curves in Fig. 1 meet.

We conclude that strong enough synaptic depression (large β) can destabilize a stationary bump that would be stable in the absence of depression. This explicitly establishes the breakdown of the Evans function approach to analyzing the stability of bump solutions of the neural field model with synaptic depression, Eq. (2.1), in the high-gain limit; the latter approach predicts that the upper branch of the existence curves in Fig. 1 is stable. However, it is important to note that the piecewise smooth approach itself can only provide sufficient conditions for instability but not stability of a bump. This follows from the fact that we had to assume that λ is real in order to construct separable solutions of the pseudo-linear Eqs. (2.23) and (2.24). Hence, there could be unstable modes corresponding to non-separable oscillatory solutions that are not picked up by our analysis, although numerical simulations suggest that this is not the case for our particular system. Finally, the piecewise smooth approach can be extended to the case of radially symmetric two-dimensional bumps, although the resulting analysis is more complicated since one has to keep track of variations in the sign of perturbations around the circular boundary of the bump [36].

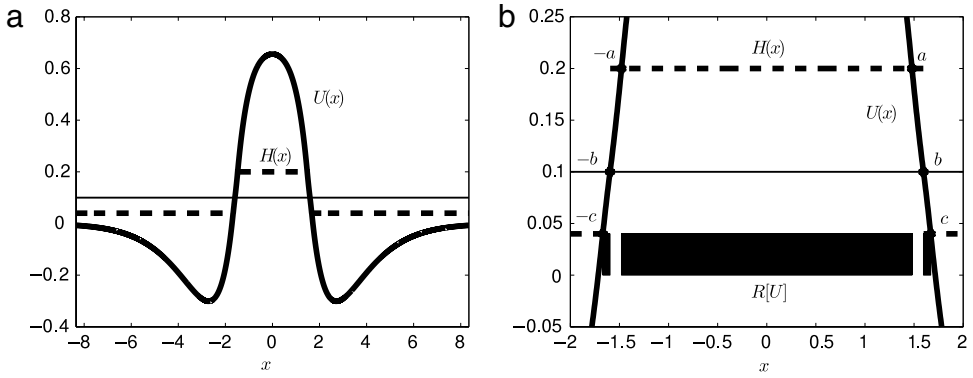

Fig. 4. Stationary bump in a network with spike frequency adaptation. (a) Bump solution $(U(x), H(x))$ with $h_0 = 0.04$, $\theta = 0.1$, and $\kappa = 0.16$. Here $a = 1.48$, $b = 1.60$, and $c = 1.67$. (b) Zoomed in version of the excited region $R[U]$, showing all of the threshold crossings at $x = \pm a, \pm b, \pm c$.
Source: Adapted from [23,25].

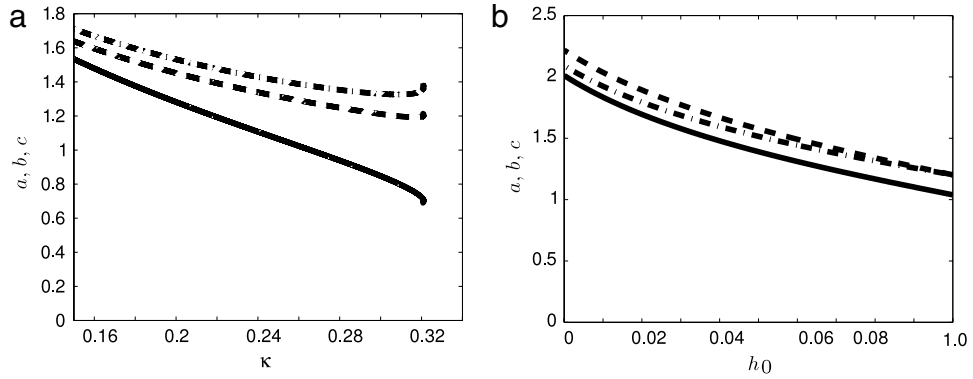

Fig. 5. (a) Plot of bump half-widths versus κ for $\theta = 0.1$ and $h_0 = 0.04$. The bump solution exists for $\kappa < \kappa_c \approx 0.32$. (b) Plot of bump half-widths versus h_0 for $\theta = 0.1$ and $\kappa = 0.16$. The bump solution exists for $h_0 > h_c \approx 0$.

3. Neural network with spike frequency adaptation

In this section, we analyze the existence and stability of stationary bumps in a neural network with spike frequency adaptation. Spike frequency adaptation is the process by which a neuron's firing rate decays to a submaximal level, occurring when a hyperpolarizing potassium current is activated via intracellular calcium [37,38]. Since increases in adaptation current are subtractive terms entering the sum total of all currents driving a population, they can be equivalently thought of as increases in the threshold required for a nonzero population firing rate. This phenomenon was recently incorporated into the scalar neural network (1.1) by introducing a dynamic threshold into the firing rate function, so that on setting $f = \Theta$ we have [23,25]

$$\frac{1}{\alpha}\frac{\partial u(x,t)}{\partial t} = -u(x,t) + \int_{-\infty}^{\infty} w(x-x')\Theta(u(x',t) - h(x',t))\mathrm{d}x', \tag{3.1a}$$

$$\frac{\partial h(x,t)}{\partial t} = -(h(x,t) - h_0) + \kappa\Theta(u(x,t) - \theta). \tag{3.1b}$$

The threshold $h(x,t)$ increases from its baseline value h_0 to a maximum of $h_0 + \kappa$, when the input drive $u(x,t)$ is above θ. In keeping with previous analyses of this model, we require the threshold parameters satisfy $h_0 < \theta < h_0 + \kappa$. However, derivations of firing rate models with spike frequency adaptation from detailed conductance based models suggest that taking $h_0 = \theta$ is more physiologically reasonable [37]. The time constant α quantifies the ratio between synaptic input dynamics and adaptation dynamics. In order to make a direct comparison with Coombes and Owen [23,25], we take a Mexican hat weight function of the form (2.5).

3.1. Existence of bumps

A stationary bump solution $(U(x), H(x))$ of (3.1) satisfies

$$U(x) = \int_{-\infty}^{\infty} w(x-x')\Theta(U(x') - H(x'))\mathrm{d}x', \tag{3.2}$$

$$H(x) = h_0 + \kappa\Theta(U(x) - H(x)). \tag{3.3}$$

We restrict ourselves to examining single bumps that satisfy the threshold conditions

$$U(\pm a) = h_0 + \kappa, \qquad U(\pm b) = \theta, \qquad U(\pm c) = h_0, \tag{3.4}$$

where $a < b < c$. As opposed to bumps in the scalar and depressing networks, the stationary bump solution here will have a disconnected excited region for U, $R[U] = (-c, -b) \cup (-a, a) \cup (b, c)$, and a different excited region for H, $R[H] = (-b, b)$ so that

$$U(x) = \left(\int_{-c}^{-b} + \int_{-a}^{a} + \int_{b}^{c}\right) w(x-x')\mathrm{d}x'. \tag{3.5}$$

An example of such a bump is shown in Fig. 4. This should be contrasted with multibump solutions, whose activity is in excess of a homogeneous threshold over several disconnected subdomains [11,12,16]. For the Mexican hat weight function (2.5), we can explicitly evaluate the integrals in (3.5) to yield

$$U(x) = g(x+c) - g(x+b) + g(x+a) - g(x-a) + g(x-b) - g(x-c), \tag{3.6}$$

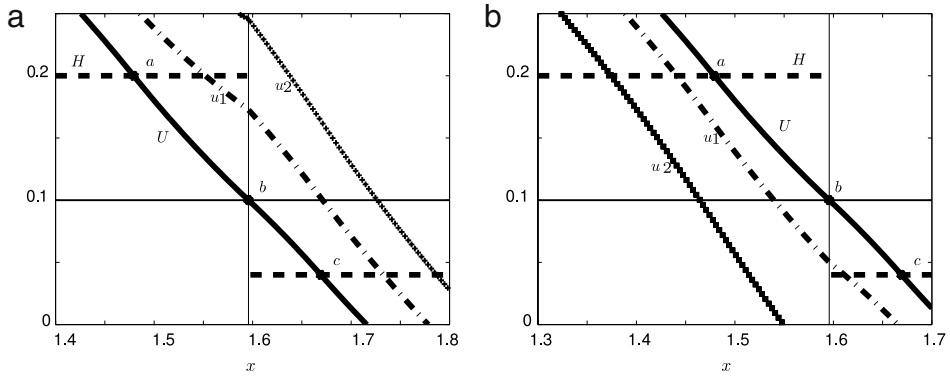

Fig. 6. Different sized perturbations of a bump. (a) Expanding a side of the bump. Zoomed-in version of the bump $(U(x), H(x))$ is shown along with perturbed solutions $u_1(x) = U(x) + \psi_1(x)$ and $u_2(x) = U(x) + \psi_2(x)$ with $\psi_i(x) > 0$. While u_1 satisfies the three threshold crossings on this side, u_2 does not, due to the condition $u_2(a + \Delta_+^a) = h_0 + \kappa$ being violated. (b) Contracting a side of the bump. Here, $u_1(x) = U(x) - \psi_1(x)$, $(\psi_1(x) > 0)$ still satisfies all three threshold crossing, but $u_2 = U - \psi_2$, $(\psi_2 > 0)$ does not, due to $u_2(c + \Delta_c^+) = h_0$ being violated. Parameters are $h_0 = 0.04, \theta = 0.1, \kappa = 0.16$.

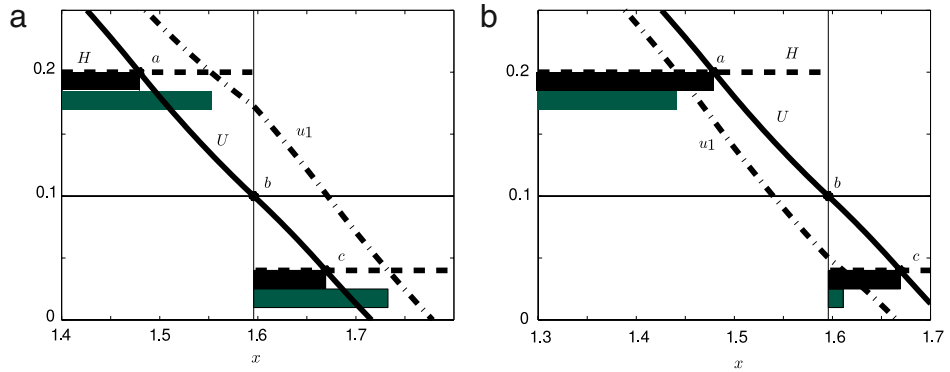

Fig. 7. Effects of perturbations on the excited region $R[U]$. (a) Zoomed-in version of the bump $U(x)$, $H(x)$ shows the accompanying excited region $R[U]$ (black bar). Expanding a side of the bump to the perturbed form $u_1(x) = U(x) + \psi_1(x)$, $(\psi_1 > 0)$ will widen both subdomains of the excited region $R[u_1]$ (grey bars). (b) Contracting a side of the bump to the perturbed form $u_1(x) = U(x) - \psi_1(x)$, $(\psi_1 > 0)$ shrinks both subdomains of the excited region $R[u_1]$ (grey bars). Parameters are $h_0 = 0.04, \theta = 0.1, \kappa = 0.16$.

where $g(x) = xe^{-|x|}$. Also note

$$H(x) = \begin{cases} h_0 + \kappa, & |x| > b, \\ h_0, & |x| < b, \end{cases} \tag{3.7}$$

implying that, as in the case of the network with depression, the negative feedback variable here will have a jump discontinuity. Applying the bump threshold conditions (3.4)–(3.6), we arrive at an implicit system relating the bump half-widths a, b, c to all other parameters

$$\begin{aligned} &g(a+c) - g(a+b) + g(2a) + g(a-b) - g(a-c) = h_0 + \kappa, \\ &g(b+c) - g(2b) + g(b+a) - g(b-a) - g(b-c) = \theta, \\ &g(2c) - g(c+b) + g(c+a) - g(c-a) + g(c-b) = h_0. \end{aligned} \tag{3.8}$$

The system of transcendental equations (3.8) can be solved numerically using a root finding algorithm. The variation of pulse width with the parameters κ and h_0 is shown in Fig. 5. The stability of the bumps is calculated below.

3.2. Stability of bumps

As in the case of networks with synaptic depression (2.1), the Evans function approach to analyzing the stability of bumps breaks down in the high-gain limit due to the vanishing small domain over which linearization is applicable. (The construction of the Evans function for traveling pulses can still be carried out, however [23,25].) Therefore, we will proceed by considering infinitesimal perturbations of the piecewise smooth system (3.1). As we show below, there are some subtle differences between the stability analysis of the system (3.1) as compared with the system (2.1). First, we will not be able to make a change of variables (2.20) in order to smooth the dynamics of the perturbation in the h variable, as we were able to do in the case of the depression variable q. Therefore, the linear stability equations we derive here will not reflect the underlying translation invariance of the system. Also, as opposed to the depression network, when bumps are unstable, linear stability of the adapting network becomes a very poor approximation to the full system's dynamics soon after perturbations begin to evolve. This is due in part to the fact that u quickly ceases to intersect h at the same number of points as the stationary solution (see Fig. 6).

Let us set $u(x,t) = U(x) + \epsilon\psi(x,t)$ and $h(x,t) = H(x) + \epsilon\varphi(x,t)$ with ψ, φ smooth perturbations and $\epsilon \ll 1$. Substituting into the full system (3.1), dividing through by ϵ and imposing the stationary bump solutions (3.2) and (3.3) gives

$$\begin{aligned} \frac{1}{\alpha}\frac{\partial\psi(x,t)}{\partial t} = -\psi(x,t) + \frac{1}{\epsilon}\int_{-\infty}^{\infty} w(x-x')\Big[\Theta(U(x') \\ + \epsilon\psi(x',t) - H(x') - \epsilon\varphi(x',t)) - \Theta(U(x') - H(x'))\Big]\mathrm{d}x' \end{aligned} \tag{3.9}$$

$$\begin{aligned} \frac{\partial\varphi(x,t)}{\partial t} = -\varphi(x,t) + \frac{\kappa}{\epsilon}[\Theta(U(x) + \epsilon\psi(x,t) - \theta) \\ - \Theta(U(x) - \theta)]. \end{aligned} \tag{3.10}$$

Denote the infinitesimal perturbations of the bump boundary for the u variable by $\epsilon\Delta_\pm^a(t), \epsilon\Delta_\pm^b(t), \epsilon\Delta_\pm^c(t)$ such that

$$u(\pm a + \epsilon\Delta_\pm^a(t), t) = h(\pm a + \epsilon\Delta_\pm^a(t), t),$$

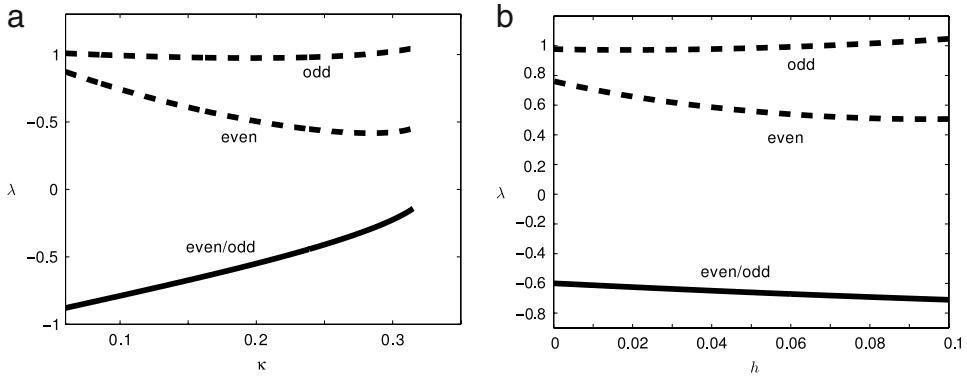

Fig. 8. Plot of eigenvalues arising from perturbations of a bump solution as a function of (a) κ with $h_0 = 0.04$, and (b) h_0 with $\kappa = 0.16$. In both plots, the positive eigenvalue associated with a shift perturbation is always larger than that associated with an expansion/contraction. Other parameters are $\theta = 0.1$ and $\alpha = 1$. Varying α has the effect of merely scaling the eigenvalues, but not changing their sign.

$$u(\pm b + \epsilon \Delta_{\pm}^{b}(t), t) = \theta, \qquad (3.11)$$
$$u(\pm c + \epsilon \Delta_{\pm}^{c}(t), t) = h(\pm c + \epsilon \Delta_{\pm}^{c}(t), t),$$

for an initial time interval following the perturbation $t \in (0, T)$. The linear theory will only be valid until the time T that the existence threshold conditions are violated. It is straightforward to Taylor expand the expressions in (3.11), truncate to first order in ϵ, and solve for the terms

$$\Delta_{\pm}^{a}(t) \approx \pm \frac{\psi(\pm a, t) - \varphi(\pm a, t)}{|U'(a)|},$$
$$\Delta_{\pm}^{b}(t) \approx \pm \frac{\psi(\pm b, t)}{|U'(b)|}, \qquad (3.12)$$
$$\Delta_{\pm}^{c}(t) \approx \pm \frac{\psi(\pm c, t) - \varphi(\pm c, t)}{|U'(c)|}.$$

It is important to note that an infinitesimal shift of the point at which u crosses θ is not equivalent to shifting the boundary of the outer region of the excited region of u, due to the discontinuity in $H(x)$. As shown in Fig. 7, infinitesimal perturbations of the bump lead to changes in the excited region of u in a neighborhood of $x = \pm a, \pm c$ but not $x = \pm b$. For the excited region of u, $R[u]$, to change in the vicinity of $x = \pm b$, it would be necessary to have an $\mathcal{O}(1)$ change in the threshold h by, for example, uniformly shifting the full bump solution. Thus, while the shift of the threshold condition near $x = \pm b$ does affect the φ dynamics, it will not affect the ψ dynamics for sufficiently small perturbations. If we now express the convolution in (3.9) in terms of the bump crossings a, b, c and perturbations $\Delta_{\pm}^{a}$, $\Delta_{\pm}^{c}$, we have

$$\frac{1}{\alpha}\frac{\partial \psi(x,t)}{\partial t} = -\psi(x,t) + \frac{1}{\epsilon}\Bigg[\int_{-c+\epsilon\Delta_{-}^{c}}^{-b} w(x-x')\mathrm{d}x' - \int_{-c}^{-b} w(x-x')\mathrm{d}x' + \int_{-a+\epsilon\Delta_{-}^{a}}^{a+\epsilon\Delta_{+}^{a}} w(x-x')\mathrm{d}x' - \int_{-a}^{a} w(x-x')\mathrm{d}x' + \int_{b}^{c+\epsilon\Delta_{+}^{c}} w(x-x')\mathrm{d}x' - \int_{b}^{c} w(x-x')\mathrm{d}x'\Bigg]. \qquad (3.13)$$

Let us now consider an initial perturbation that only changes the activity variable u, that is, $\varphi(x, 0) = 0$ for all x. We can then linearize the integral terms in Eq. (3.13) by only keeping terms up to first order in the perturbations ψ, $\Delta_{\pm}^{x}$, since $\varphi(\pm a, t) = 0 = \varphi(\pm c, t)$ within the linear regime, that is, infinitesimal changes in u will only perturb the threshold in a neighborhood of $x = \pm b$. Thus,

$$\frac{1}{\epsilon}\int_{-c+\epsilon\Delta_{-}^{c}}^{-c} w(x-x')\mathrm{d}x' \approx -\Delta_{-}^{c} w(x+c) \approx \gamma_c w(x+c)\psi(-c,t), \qquad (3.14)$$
$$\frac{1}{\epsilon}\int_{-a+\epsilon\Delta_{-}^{a}}^{-a} w(x-x')\mathrm{d}x' \approx -\Delta_{-}^{a} w(x+a) \approx \gamma_a w(x+a)\psi(-a,t), \qquad (3.15)$$
$$\frac{1}{\epsilon}\int_{a}^{a+\epsilon\Delta_{+}^{a}} w(x-x')\mathrm{d}x' \approx \Delta_{+}^{a} w(x-a) \approx \gamma_a w(x-a)\psi(a,t), \qquad (3.16)$$
$$\frac{1}{\epsilon}\int_{c}^{c+\epsilon\Delta_{+}^{c}} w(x-x')\mathrm{d}x' \approx \Delta_{+}^{c} w(x-c) \approx \gamma_c w(x-c)\psi(c,t), \qquad (3.17)$$

where $\gamma_y^{-1} = |U'(y)|$. This yields the linear equation

$$\frac{1}{\alpha}\frac{\partial \psi(x,t)}{\partial t} = -\psi(x,t) + \gamma_a(w(x+a)\psi(-a,t) + w(x-a)\psi(a,t)) + \gamma_c(w(x+c)\psi(-c,t) + w(x-c)\psi(c,t)). \qquad (3.18)$$

Assuming separability $\psi(x,t) = \mathrm{e}^{\lambda t}\psi(x)$, we derive a spectral equation that determines the linear stability of a bump solution with respect to the given restricted class of perturbations:

$$(\lambda+\alpha)\psi(x) = \alpha\gamma_a(w(x+a)\psi(-a) + w(x-a)\psi(a)) + \alpha\gamma_c(w(x+c)\psi(-c) + w(x-c)\psi(c)). \qquad (3.19)$$

Note that Eq. (3.19) is a modified version of the spectral equation for the scalar Amari equation [6]. The dynamic threshold introduces extra threshold crossing points that appear as additional pointwise terms. This is equivalent to the spectral equation one would derive for an Amari network with a spatially inhomogeneous threshold, specified by $H(x)$. Therefore, the translation invariance of the bump will no longer be implied by the linear stability equation, since translations of $H(x)$ would involve $\mathcal{O}(1)$ additions, which we must exclude from our analysis, based on our assumption that $\varphi(x)$ remains small. The linear operator on the right-hand side of Eq. (3.19) has an essential spectrum located at $\lambda = -\alpha$ and a discrete spectrum that is obtained by setting $x = \pm a, \pm c$. The latter yields the following matrix equation for $\bar{\psi} = (\psi(-a), \psi(a), \psi(-c), \psi(c))^T$:

$$\lambda\bar{\psi} = \alpha(\mathbf{M} - I_4)\bar{\psi}, \quad \text{where}$$

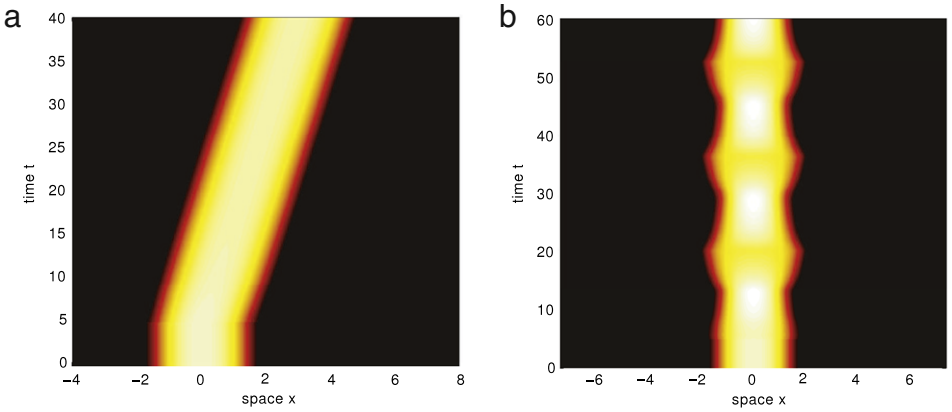

Fig. 9. Instabilities of a stationary bump solution given by Eqs. (3.6) and (3.7). (a) Space–time plot of a bump destabilizing to form a traveling pulse for $\alpha = 1.0$, $\kappa = 0.16$. The activity $u(x, t)$ evolves from an initial bump solution that is perturbed by a small rightward shift at $t = 5$. (b) Space–time plot of a bump destabilizing to form a spatially localized breather for $\alpha = 1.2$, $\kappa = 0.16$. The activity $u(x, t)$ evolves from an initial bump solution that is perturbed by an expansion at $t = 5$. Other parameters are $\theta = 0.1$, $h_0 = 0.04$.

$$\mathbf{M} = \begin{pmatrix} \gamma_a w(0) & \gamma_a w(2a) & \gamma_c w(c-a) & \gamma_c w(a+c) \\ \gamma_a w(2a) & \gamma_a w(0) & \gamma_c w(a+c) & \gamma_c w(c-a) \\ \gamma_a w(c-a) & \gamma_a w(a+c) & \gamma_c w(0) & \gamma_c w(2c) \\ \gamma_a w(a+c) & \gamma_a w(c-a) & \gamma_c w(2c) & \gamma_c w(0) \end{pmatrix}, \tag{3.20}$$

where I_n is the $n \times n$ identity matrix. Let us define an even (odd) eigenmode as one for which $\psi(x) = \psi(-x)$ ($\psi(x) = -\psi(-x)$) at $x = a, c$. An even eigenmode corresponds to an expansion/contraction of the bump, whereas an odd eigenmode corresponds to a shift of the bump. For all parameter values that we have explored, we find that there are two positive eigenvalues, with the larger (smaller) positive eigenvalue corresponding to an odd (even) eigenmode, and a degenerate negative eigenvalue with an even/odd pair of eigenmodes. By applying the ansatz of an eigenmode being even or odd, we can compute these eigenvalues analytically by evaluating the roots of a quadratic. In the case of even eigenmodes, the associated pair of eigenvalues is

$$\lambda_{\pm}^{\mathrm{e}} = \frac{\alpha}{2}\left(\gamma_a \Omega_+^a + \gamma_c \Omega_+^c - 2 \pm \sqrt{(\gamma_a \Omega_+^a - \gamma_c \Omega_+^c)^2 + 4\gamma_a\gamma_c \left(\Omega_+^m\right)^2}\right), \tag{3.21}$$

and in the case of odd eigenmodes, the associated pair of eigenvalues is

$$\lambda_{\pm}^{\mathrm{o}} = \frac{\alpha}{2}\left(\gamma_a \Omega_-^a + \gamma_c \Omega_-^c - 2 \pm \sqrt{(\gamma_a \Omega_-^a - \gamma_c \Omega_-^c)^2 + 4\gamma_a\gamma_c \left(\Omega_-^m\right)^2}\right), \tag{3.22}$$

where

$$\Omega_{\pm}^a = w(0) \pm w(2a), \qquad \Omega_{\pm}^c = w(0) \pm w(2c), \qquad \Omega_{\pm}^m = w(c-a) \pm w(c+a). \tag{3.23}$$

The dependence of the eigenpairs (3.21) and (3.22) on parameters is illustrated in Fig. 8. Clearly, varying α will not change the sign of the eigenvalues λ and thus the qualitative linear stability of bumps. In contrast to our analysis, the Evans function approach predicts that bumps are stable for sufficiently small α [23,25] but destabilize to form a traveling pulse or breather as α increases. However, numerical simulations of the full system (3.1) confirm that bumps are always unstable. Moreover, the qualitative behavior of the resulting instabilities are consistent with our piecewise smooth analysis (see below).

3.3. Numerical simulations

We now study the full system (3.1) using a numerical approximation scheme. To evolve the system in time, we use a fourth order Runge–Kutta method with 2000–4000 spatial grid points and a time-step of $dt = 0.01$. The integral term in Eq. (3.1a) is approximated using Simpson's rule. For all of our numerical simulations, we begin with an initial condition $u(x, 0)$ given by an exact bump solution specified by Eqs. (3.6) and (3.7). After a brief period, we perturb the system according to $u(x) \to u(x) + \psi_{\pm}(x)$ with

$$\psi_{\pm}(x) = \chi\left(w(x+a) \pm w(x-a) + w(x+c) \pm w(x-c)\right), \tag{3.24}$$

and observe how the system then evolves. Leftward shifts (rightward shifts) correspond to $\psi_-(x, t)$ when $\chi \geq 0$ ($\chi \leq 0$), while expansions (contractions) correspond to $\psi_+(x, t)$ when $\chi \geq 0$ ($\chi \leq 0$). Note that the perturbation $\psi_+(x)(\psi_-(x))$ is a mixture of even (odd) eigenmode solutions of Eq. (3.19). The resulting dynamics depends specifically on the type of perturbation applied to the bump. For each simulation, we systematically examined whether or not taking finer grids changed the stability results. We found that as the grid spacing was decreased the size of perturbation necessary to destabilize the bump also decreased. This is important because too coarse a grid can drastically alter numerical results, since discreteness can stabilize bumps that are not stable in the continuous system [35].

When shift perturbations destabilize the bump, the resulting dynamics evolves to a traveling pulse solution, as illustrated in Fig. 9(a) for a rightward shift. Coombes and Owen [23,25] have shown that spike frequency adaptation can indeed generate stable traveling pulses for a wide range of parameters in the system (3.1). Following a perturbation by a rightward shift, the nonlinear threshold initially decays at what becomes the trailing edge of the pulse. As the leading edge moves rightward as well, the structure soon propagates invariantly, as demonstrated by the time snapshots in Fig. 10. In other simulations, we found that increasing α leads to faster traveling pulses and therefore a more obvious initial destabilization, in good agreement with the linear theory. In Fig. 9(b), we show an example of how an expansion destabilizes a bump leading to the formation of a breather, the existence of which was previously established by Coombes and Owen [23,25]. A closer look at the corresponding snapshots in Fig. 11 shows that the

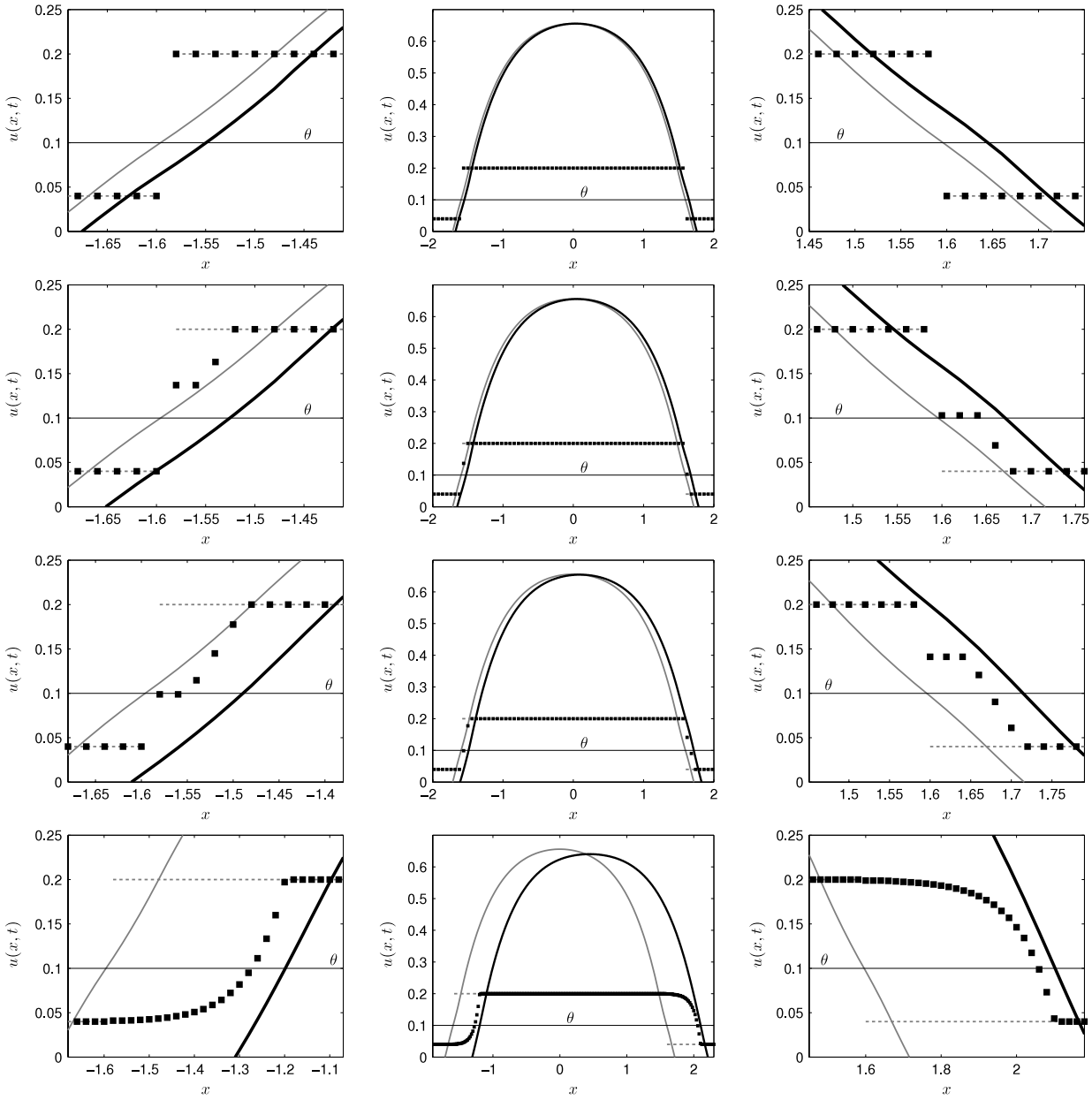

Fig. 10. Snapshots of a bump destabilizing to a traveling pulse at successive times $t = 5, 5.5, 6, 10$ (top to bottom) for $\alpha = 1.0$, and $\kappa = 0.16$. Both $u(x, t)$ (solid black curves) and $h(x, t)$ (black squares) are shown in full view (center column), at the trailing edge (left column), and at the leading edge (right column). Also shown are the initial conditions of the bump for $U(x)$ (solid grey curve) and $H(x)$ (dashed grey curve). Eventually, the threshold crossings $u(a + \Delta_+^a, t) = h_0 + \kappa$ and $u(-c + \Delta_-^c, t) = h_0$. Other parameters are $h_0 = 0.04$, $\theta = 0.1$.

breather begins contracting once the threshold h becomes higher in amplitude than u at the pulse edge. The oscillation amplitude of the breathing solution decreases as α decreases. Finally, in Fig. 12 we show an example of a shift perturbation destabilizing a bump in the case of stronger adaptation (larger κ). In this case the traveling pulse crosses threshold at five locations, rather than four points as in Fig. 10.

4. Discussion

In this paper we analyzed the linear stability of stationary bumps in a piecewise smooth neural field model with either synaptic depression or spike frequency adaptation. In both cases, stability analysis based on the construction of an Evans function breaks down in the high-gain limit. In the case of synaptic depression, we found that sufficiently strong synaptic depression can destabilize a bump that would be stable in the absence of synaptic depression; instabilities are dominated by shift perturbations that evolve into traveling pulses. The stability analysis assumed that the dominant instabilities were associated with non-oscillatory, separable solutions of the pseudo-linear Eqs. (2.23) and (2.24). However, there are well known scenarios in neural field models where Hopf bifurcations can occur leading to spatially structured oscillations such as breathers and target patterns [19,14,15,24]. In future work it would be interesting to analyze generalized Hopf bifurcations in neural field models with nonlinear forms of adaptation such as synaptic depression, along the lines of recent studies of nonsmooth dynamical systems [28, 39]. In the case of spike frequency adaptation, we found that bumps are always unstable, and that destabilization of a bump can result in either a traveling pulse or a spatially localized breather. In future work it would be interesting to develop tools to analyze the nonlinear (order one) instabilities of the adaptive network (3.1). This would allow us to analytically find

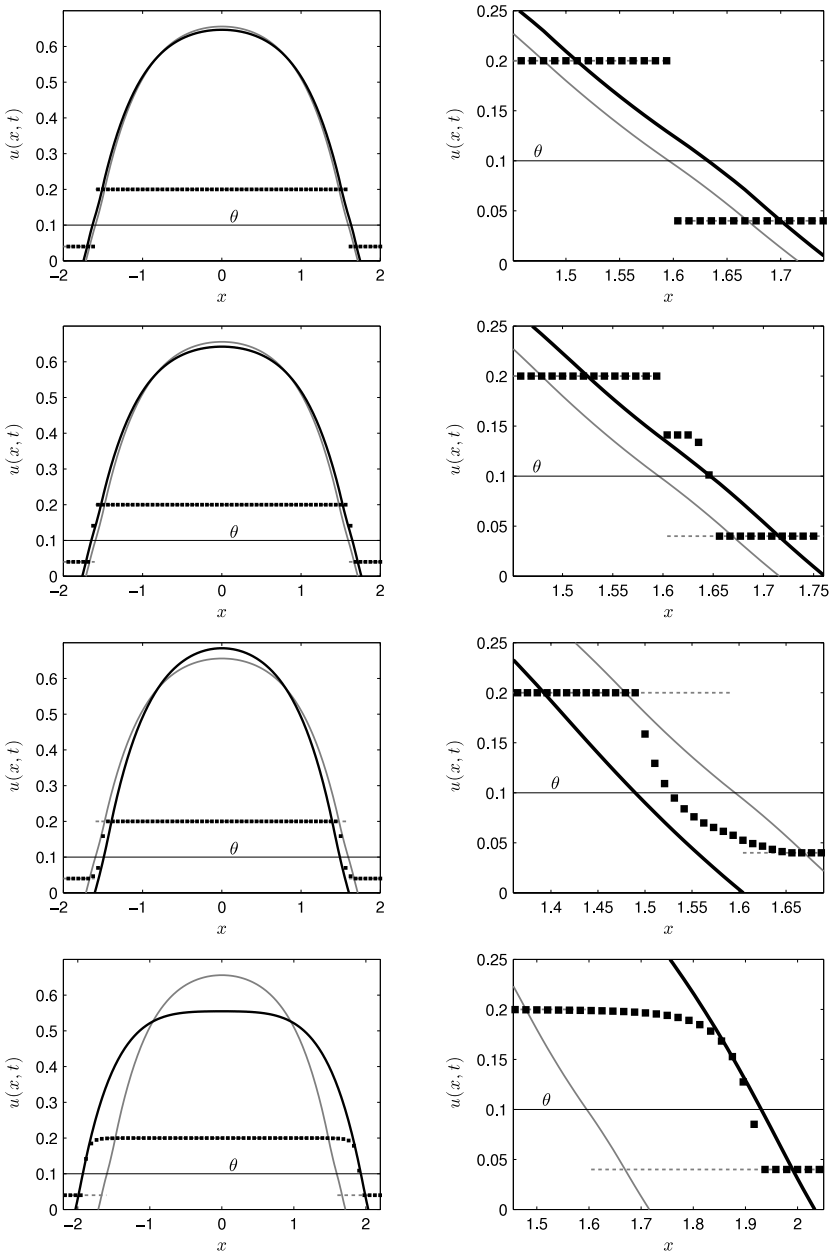

Fig. 11. Snapshots of a bump destabilizing to a breather at successive times $t = 5, 6, 10, 20$ (top to bottom) for $\alpha = 1.2$ and $\kappa = 0.16$. Both $u(x, t)$ (black curves) and $h(x, t)$ (solid black squares) are shown in full view (left column), and for the right-hand side of the bump (right column). Also shown are the initial conditions of the bump for $U(x)$ (solid grey curve) and $H(x)$ (dashed grey curve). The threshold crossings $u(\pm a + \Delta_{\pm}^{a}, t) = h_0 + \kappa$ and $u(\pm c + \Delta_{\pm}^{c}, t) = h_0$ periodically vanish. Other parameters are $h_0 = 0.04, \theta = 0.1$.

the period of oscillation in the breathing solutions identified using numerics.

Finally, it could be argued that analyzing the dynamics of networks with Heaviside nonlinearities is not very realistic from a neurobiological perspective, and introduces unnecessary mathematical complications compared to smooth firing rate functions. However, following the original analysis of Amari [6], there have been many studies of neural field models where taking the high-gain limit of a sigmoid function has provided a useful framework for constructing explicit stationary and traveling wave solutions (as reviewed in [9]). This constructive approach has been particularly useful in providing qualitative insights into how spatiotemporal network dynamics depends on the structure of the synaptic weight kernel. Moreover, in certain cases it is possible to use singular perturbation methods [22,19] or fixed point theorems [18,40] to extend results for networks with Heaviside nonlinearities to those with sigmoidal nonlinearities. The analysis presented in this paper shows that the high-gain limit becomes singular when nonlinear forms of adaptation are incorporated into neural field models, and suggests that stable bump solutions found in such networks with smooth nonlinearities either become unstable or develop vanishingly small basins of attraction as the gain of the sigmoid increases.

Acknowledgements

We thank Steve Coombes and Markus Owen for helpful comments clarifying the specifics of their papers [23,25]. This publication was based on work supported in part by the National Science Foundation (DMS-0813677) and by Award

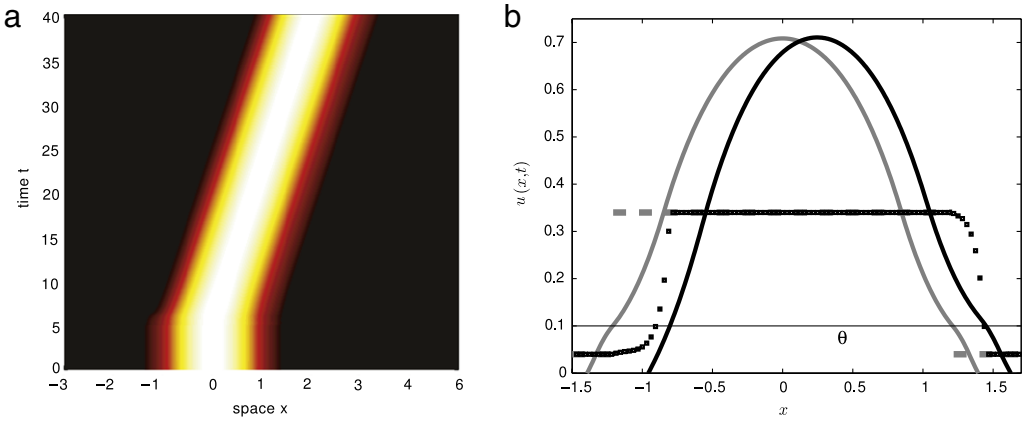

Fig. 12. Bump destabilizing to a traveling pulse for $\alpha = 2.0$, $\kappa = 0.3$. (a) Space–time plot of the activity $u(x, t)$ evolving from an initial bump solution that is perturbed by a small rightward shift at $t = 5$. (b) Snapshot of perturbed solution $u(x, t)$ (black solid curve) and $h(x, t)$ (black squares) at time $t = 20$, along with initial profiles $U(x)$ (grey curve) and $H(x)$ (grey dashed curve). Eventually, the threshold crossing $u(a + \Delta_+^a, t) = h_0 + \kappa$ vanishes. Other parameters are $h_0 = 0.04$, $\theta = 0.1$.

No. KUK-C1-013-4 granted by King Abdullah University of Science and Technology (KAUST). PCB was also partially supported by the Royal Society Wolfson Foundation.

References

[1] S. Funahashi, C.J. Bruce, P.S. Goldman-Rakic, Mnemonic coding of visual space in the monkey's dorsolateral prefrontal cortex, J. Neurophysiol. 61 (2) (1989) 331–349.
[2] E.K. Miller, C.A. Erickson, R. Desimone, Neural mechanisms of visual working memory in prefrontal cortex of the macaque, J. Neurosci. 16 (1996) 5154–5167.
[3] X.J. Wang, Synaptic reverberation underlying mnemonic persistent activity, Trends Neurosci. 24 (8) (2001) 455–463.
[4] H.S. Seung, How the brain keeps the eyes still, Proc. Natl. Acad. Sci. USA 93 (1996) 13339–13344.
[5] R. Ben-Yishai, R.L. Bar-Or, H. Sompolinsky, Theory of orientation tuning in visual cortex, Proc. Natl. Acad. Sci. USA 92 (1995) 3844–3848.
[6] S. Amari, Dynamics of pattern formation in lateral-inhibition type neural fields, Biol. Cybernet. 27 (2) (1977) 77–87.
[7] X.J. Wang, Synaptic basis of cortical persistent activity: the importance of NMDA receptors to working memory, J. Neurosci. 19 (21) (1999) 9587–9603.
[8] C.R. Laing, C.C. Chow, Stationary bumps in networks of spiking neurons, Neural Comput. 13 (2001) 1473–1494.
[9] S. Coombes, Waves, bumps, and patterns in neural field theories, Biol. Cybernet. 93 (2) (2005) 91–108.
[10] S. Coombes, M.R. Owen, Evans functions for integral neural field equations with heaviside firing rate function, SIAM J. Appl. Dyn. Syst. 34 (2004) 574–600.
[11] C.R. Laing, W.C. Troy, B. Gutkin, G.B. Ermentrout, SIAM J. Appl. Math. 63 (1) (2002) 62–67.
[12] C.R. Laing, W.C. Troy, PDE methods for nonlocal models, SIAM J. Appl. Dyn. Syst. 2 (3) (2003) 487–516.
[13] H. Werner, T. Richter, Circular stationary solutions in two-dimensional neural fields, Biol. Cybernet. 85 (2001) 211–217.
[14] S.E. Folias, P.C. Bressloff, Breathing pulses in an excitatory neural network, SIAM J. Appl. Dyn. Syst. 3 (3) (2004) 378–407.
[15] S.E. Folias, P.C. Bressloff, Breathers in two-dimensional neural media, Phys. Rev. Lett. 95 (20) (2005) 208107.
[16] M.R. Owen, C.R. Laing, S. Coombes, Bumps and rings in a two-dimensional neural field: splitting and rotational instabilities, New J. Phys. 9 (2007) 378.
[17] P.C. Bressloff, Weakly interacting pulses in synaptically coupled excitable neural media, SIAM J. Appl. Math. 66 (2005) 57–81.
[18] K. Kishimoto, S. Amari, Existence and stability of local excitations in homogeneous neural fields, J. Math. Biol. 7 (1979) 303–318.
[19] D.J. Pinto, G.B. Ermentrout, Spatially structured activity in synaptically coupled neuronal networks: II. Lateral inhibition and standing pulses, SIAM J. Appl. Math. 62 (1) (2001) 226–243.
[20] O. Faugeras, R. Veltz, F. Grimbert, Persistent neural states: stationary localized activity patterns in nonlinear continuous n-population, q-dimensional neural networks, Neural Comput. 21 (2009) 147–187.
[21] J.-Y. Wu, Propagating waves of activity in the neocortex: what they are, what they do, Neuroscientist 14 (5) (2008) 487–502.
[22] D.J. Pinto, G.B. Ermentrout, Spatially structured activity in synaptically coupled neuronal networks: I. Traveling fronts and pulses, SIAM J. Appl. Math. 62 (1) (2001) 206–225.
[23] S. Coombes, M.R. Owen, Bumps, breathers, and waves in a neural network with spike frequency adaptation, Phys. Rev. Lett. 94 (14) (2005) 148102.
[24] W.C. Troy, V. Shusterman, Patterns and features of families of traveling waves in large-scale neuronal networks, SIAM J. Appl. Dyn. Syst. 6 (1) (2007) 263–292.
[25] S. Coombes, M.R. Owen, Exotic dynamics in a firing rate model of neural tissue with threshold accomodation, AMS Contemp. Math. 440 (2007) 123–144.
[26] Z.P. Kilpatrick, P.C. Bressloff, Effects of synaptic depression and adaptation on spatiotemporal dynamics of an excitatory neuronal network, Physica D (2009) (in press).
[27] Z.P. Kilpatrick, P.C. Bressloff, Spatially structured oscillations in a two-dimensional excitatory neuronal network with synaptic depression, J. Comput. Neurosci. (2009) (in press).
[28] M. Di Bernardo, C.J. Budd, A.R. Champneys, Bifurcations in nonsmooth dynamical systems, SIAM Rev. 50 (2008) 629–701.
[29] R.S. Zucker, W.G. Regehr, Short-term synaptic plasticity, Annu. Rev. Physiol. 64 (2) (2002) 355–405.
[30] M. Tsodyks, K. Pawelzik, H. Markram, Neural networks with dynamic synapses, Neural Comput. 10 (4) (1998) 821–835.
[31] J. Tabak, W. Senn, M.J. O'Donovan, J. Rinzel, Modeling of spontaneous activity in developing spinal cord using activity-dependent depression in an excitatory network, J. Neurosci. 20 (8) (2000) 3041–3056.
[32] L.F. Abbott, J.A. Varela, K. Sen, S.B. Nelson, Synaptic depression and cortical gain control, Science 275 (5297) (1997) 220–224.
[33] M.V. Tsodyks, H. Markram, The neural code between neocortical pyramidal neurons depends on neurotransmitter release probability, Proc. Natl. Acad. Sci. USA 94 (2) (1997) 719–723.
[34] Y. Guo, C.C. Chow, Existence and stability of standing pulses in neural networks: I. Existence, SIAM J. Appl. Dyn. Syst. 4 (2) (2005) 217–248.
[35] Y. Guo, C.C. Chow, Existence and stability of standing pulses in neural networks: II. Stability, SIAM J. Appl. Dyn. Syst. 4 (2) (2005) 249–281.
[36] P.C. Bressloff, Z.P. Kilpatrick, Two-dimensional bumps in a piecewise smooth neural field model with synaptic depression (2009) (submitted for publication).
[37] J. Benda, A.V.M. Herz, A universal model for spike-frequency adaptation, Neural Comput. 15 (11) (2003) 2523–2564.
[38] M. Stocker, M. Krause, P. Pedarzani, An apamin-sensitive Ca^{2+}-activated K^+ current in hippocampal pyramidal neurons, Proc. Natl. Acad. Sci. USA 96 (8) (1999) 4662–4667.
[39] Y. Zou, T. Kupper, W.J. Beyn, Generalized hopf bifurcation for planar filippov systems continuous at the origin, J. Nonlinear Sci. 16 (2006) 159–177.
[40] G.B. Ermentrout, J.B. Mcleod, Existence and uniqueness of traveling waves for a neural network, Proc. Roy. Soc. Edinburgh Sect. A 123 (1993) 461–478.